Attachment II

USC AME Report 9-11-2001

An experimental study of sonic boom penetration under a wavy air-water interface

Adam Fincham & Tony Maxworthy

University of Southern California
Aerospace and Mechanical Engineering Department
Los Angeles CA, 90089-1191, USA

Prepared for

HKC Research
Los Angeles, CA

Missile Defense Agency (MDA)
Office of Secretary of Defense

Space & Missile Systems Center (SMC)
Los Angeles AFB, CA

PARSONS
Pasadena, CA

Report Documentation Page

Form Approved
OMB No. 0704-0188

1. REPORT DATE	2. REPORT TYPE	3. DATES COVERED
APR 2002		**-**

4. TITLE AND SUBTITLE	5a. CONTRACT NUMBER
An experimental Study of Sonic Boom Penetration Under a Wavy Air-water Interface	5b. GRANT NUMBER
	5c. PROGRAM ELEMENT NUMBER
6. AUTHOR(S)	5d. PROJECT NUMBER
	5e. TASK NUMBER
	5f. WORK UNIT NUMBER
7. PERFORMING ORGANIZATION NAME(S) AND ADDRESS(ES) **Space and Missile Systems Center (SMC),Los Angeles AFB,CA,90009**	8. PERFORMING ORGANIZATION REPORT NUMBER
9. SPONSORING/MONITORING AGENCY NAME(S) AND ADDRESS(ES)	10. SPONSOR/MONITOR'S ACRONYM(S)
	11. SPONSOR/MONITOR'S REPORT NUMBER(S)

12. DISTRIBUTION/AVAILABILITY STATEMENT
Approved for public release; distribution unlimited

13. SUPPLEMENTARY NOTES
The original document contains color images.

14. ABSTRACT
see report

15. SUBJECT TERMS

16. SECURITY CLASSIFICATION OF:			17. LIMITATION OF ABSTRACT	18. NUMBER OF PAGES	19a. NAME OF RESPONSIBLE PERSON
a. REPORT	b. ABSTRACT	c. THIS PAGE			
unclassified	**unclassified**	**unclassified**		**27**	

Summary

A laboratory experiment was designed and performed to ascertain the difference in underwater response to sonic boom laboratory between flat and wavy surface models and their depth-dependent rule overpressure attenuation. Waveforms of overpressure were recorded in a water-filled tank, fitted with a surface-wave maker, during over-flight of the supersonic projectiles.

Sawyers' (1968) theory for the flat interface has been validated to a depth of at least four signature lengths. The theory of Cheng and Lee (2000) for a wavy surface has been confirmed in several respects. Firstly, the predicted overpressure attenuation with depth to the one-half power has been found to be correct over depths up to four signature lengths. Secondly, the predicted frequencies and the fore-to-aft frequency shift have been confirmed by these laboratory-scale experiments.

1. Introduction

Based on the theory of Cheng & Lee (2000) a relatively rapid program of experimental validation was initiated. The primary objective is to find the theorized effects in the laboratory and subsequently map the appropriate parameter space.

2. Laboratory Facility

Due to the implicitly dangerous nature of the experiments, they were carried out in a specially constructed acoustically damped room inside a larger experimental facility. This laboratory was specifically constructed for hypersonic projectile experiments in the late 50's and is located in a basement room with 18 inch thick concrete walls. The specially constructed acoustical chamber measures 16 x 12 x 8 feet and has lead sheet foam sandwich walls and roof, its effectiveness permitted testing with no significant noise disturbance outside of the laboratory. The inside walls of the chamber were lined with acoustic absorbing/diffusing foam that reduces any extraneous shock reflections that could interfere with the measurements.

A Plexiglas tank measuring 96 x 17 x 22 inches was lined with open-cell acoustical absorbing foam and mounted onto an optical table equipped with pneumatic vibration absorbing supports. The tank was housed in the acoustical chamber and separated from the launch device by a 6 inch thick foam filled wooden wall. A small projectile sized hole in the separating wall permits passage of the projectile while restricting the blast associated with each launch from contaminating the measurements. The distance between the launcher and the wall was chosen so as to ensure that the projectile had already escaped from the launch associated blast wave before it entered the hole in the wall. A fast Darlington type phototransistor fitted inside the wall provided consistent accurate triggering capabilities for each run, allowing the position of the projectile to be known throughout the course of its relatively short flight.

Pointed tip, blunt tail projectiles of diameter 7.7 mm and length 30 mm were fired from a rigidly mounted launcher and collected in a sand filled steel box of dimensions 24 x 19 x 10 inches. The launcher/collector combination was carefully aligned and tested then fixed permanently in place where it was left for the duration of the experiments. Changes in the mis-distance (distance from the flight path to the water surface) could be made by raising or lowering the tank. The launch velocity was measured at 2300 fps corresponding to a Mach number M_A=2.02 for the laboratory conditions and was found to vary

less than 0.3% between runs. Both the projectile size and velocity were kept constant for all experiments. The mis-distance was kept at 13.5 inches for all of the data presented here.

Quasi-2D surface capillary-gravity waves were generated by two different wave-generating systems. The first consisted of a span-wise wedge shaped paddle that was oscillated vertically through direct mechanical coupling to a pair of moving-coil actuators (speakers). The paddle was located downstream of the measurement location but due to the fall off in surface wave amplitude away from the paddle, it was necessary to position the acoustic sensors relatively close to the point of wave generation and adverse effects due to shock reflections from the part of the paddle above the water were detected. These effects limited the placement of the sensors to a minimum of 10 inches in front of the paddle, at a location where the surface wave amplitude was marginal. A second wave-generator was constructed from a simple hinged strip of polycarbonate measuring 0.75 x 21 x 1/16 inches glued to a 1/8 inch diameter titanium rod. The entire mechanism was located just under the water surface and was actuated through a slightly more elaborate system of mechanical coupling. This second generation wave-generator was found to be almost invisible to the shock (as it was physically located beneath the water surface and had an acoustic impedance close to that of the water) and was also capable of producing larger amplitude surface waves, this system was favorable and was used for all experiments subsequent to its development. The paddle could be driven with any arbitrary waveform and was capable of a maximum excursion of 7 mm peak-peak. Figure 1 shows a perspective view of the basic laboratory setup.

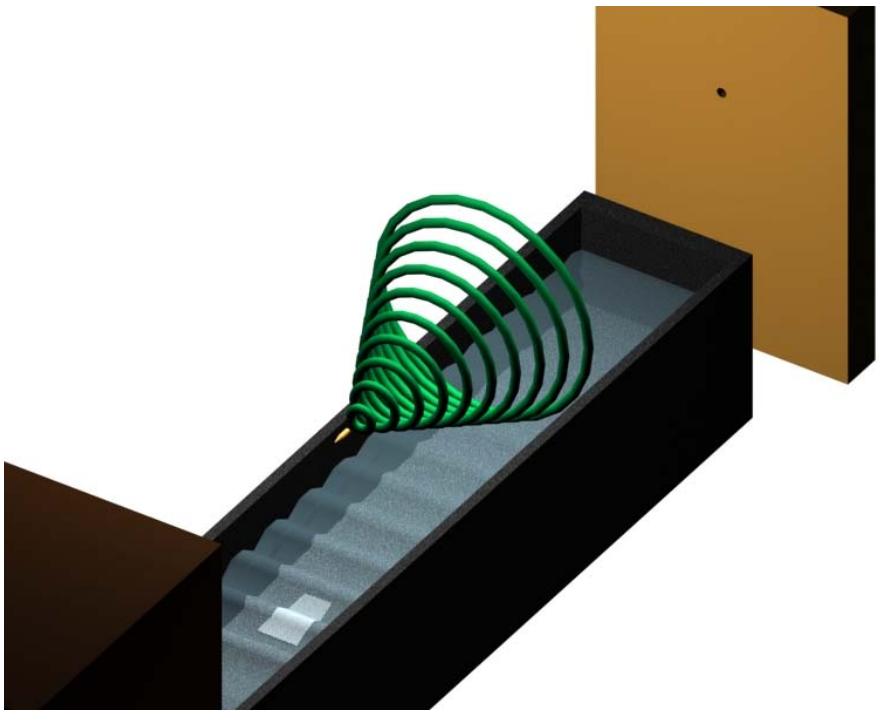

Figure 1. Perspective view of the basic laboratory setup.

All pressure measurements were made with Kistler model 211B4 and/or 211B5 type piezotron sensors with resonant frequencies of 500 and 300 kHz respectively. The piezotrons were powered by a Kistler model 5124A1 charge coupler equipped with filters in the 30-250 kHz range as was determined appropriate based on the analysis of preliminary results, a single unfiltered channel was left in all runs so that any unpredicted high frequency effects would not be lost. The transducers were flush mounted into a

5/16 inch thick Plexiglas plate of width 2 inches using Kistler model 221A sensor mounting kits. Five sensors were typically used across the span with a spacing of 2 inches. The flush plate mounting was used as it eliminated any "edge" effects caused by refraction at the borders of the sensing elements, the sensors were mounted a distance of ¾ inches from the leading edge of the Plexiglas strip. Kistler model 1635A cables were used to couple the piezotrons to the charge amplifier, a silicone heat-shrink arrangement ensured proper waterproofing of the submerged connections. The plate containing the sensors was secured to a Plexiglas frame with several steps located at known vertical depths. The frame was fixed to the floor of the tank with absorbent foam mounts and lead weights. The entire array of sensors could then be lowered or raised as a group with no changes to the water depth by simply changing the step locations (this is in contrast to the experiments of Intrieri & Malcolm (1973) where the sensors were fixed and the depth changed by added or subtracting water to/from the tank.) in this way the distance from the flight path to the water surface was kept constant ensuring the same surface forcing for each run. All data was sampled at either 245 or 600 kHz using a National Instruments model PCI-MIO-16E data acquisition board driven by a custom LabView program capable of acquiring pre-trigger data at up to 1.25 Mhz. The pre-trigger acquisition feature enabled the measurement of any launch-associated vibration such as those transmitted through the concrete floor into the tank before the arrival of the projectile.

3. Measurements and some Results

A standardized testing procedure was introduced to ensure both good repeatability and to improve on the overall safety of the experiments. The data acquisition computer and charge-coupler were run on batteries to avoid line noise in the data. All other unnecessary electronics were switched off during data acquisition to help ensure an electrically quite environment. All test were repeated at least twice to ensure repeatability and as progressive improvements to the laboratory setup were made older data was shelved in favor of the newer results. Some typical pressure signatures just above the surface of the water are shown in Figure 2. It can be seen that the incident wave signature is asymmetric due to the blunt rear of the projectile and the relatively close proximity of the measurements to the flight path. This asymmetry will be commented on later as it was thought that it may effect the downstream side of the measured underwater overpressure signals. The speed of the projectile was measured at the testing location by fitting 2 piezotrons into a Plexiglas plate with a precisely known longitudinal distance between them and placing the plate on the axis of the tank just above the surface of the water, the sharp signature characterized in Figure 2 provided a sufficiently accurate measurement of the projectile speed. Due to ballistic constraints that limited any significant variation in the projectile speed it was decided to keep this constant for all experiments. Similar data was used to calculate the length scale (L´) of the N-wave signature hitting the surface of the water. L´ was measured as the distance from the positive and negative pressure peaks of the N-wave and was found to be 8.05 cm. Although the flight time from launcher to collector was less than 6 msec data was collected from 8 msec before the launch till 12 msec after the launch. The pre-trigger data was used to examine pre-launch ambient noise levels while the data collected after the projectile entered the collector box allowed examination of the large amplitude ringing modes related to the tank geometry that result from the overall excitation of the tank/room.

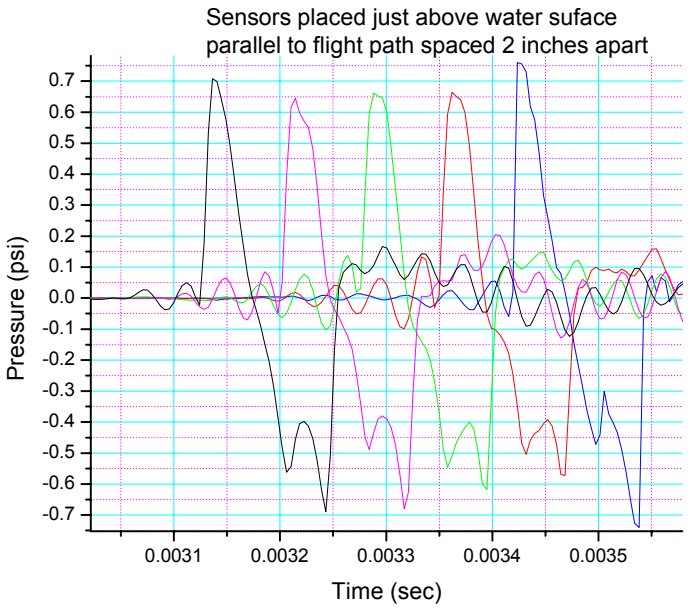

Figure 2: Pressure signals from 5 piezotrons in the air just above the air-water interface.

3.1 Flat water surface

In order to characterize the impacting wave signature and to re-verify experimentally both the Sawyer model and the Prandtl-Glauert rule, a large number of tests were done with a flat air-water interface. Most initial testing was aimed at verifying the repeatability of the incident wave in the air and at optimizing the tank/wave-generator geometry so as to eliminate or minimize any reflected/refracted shock effects.

An Initial series of tests were performed to examine the effects of depth on the over-pressure attenuation. Measurements corresponding to the far–field attenuation were made at depths of 3.4, 8.1, 15.9, 24.1, and 29.9 cm all tests were repeated twice. The resulting peak-peak over pressure verses depth plot is shown in Figure 3. The data in Figure 3 shows z^{-2} type attenuation to depths of 3.6L´, far deeper than any previously published study (Desharnais & Chapman (1998), Intrieri & Malcolm (1973), Waters & Glass (1970) and Sohn, et al (2000)) and for the first time verifies the Sawyer model experimentally for depths significantly greater than one signature length.

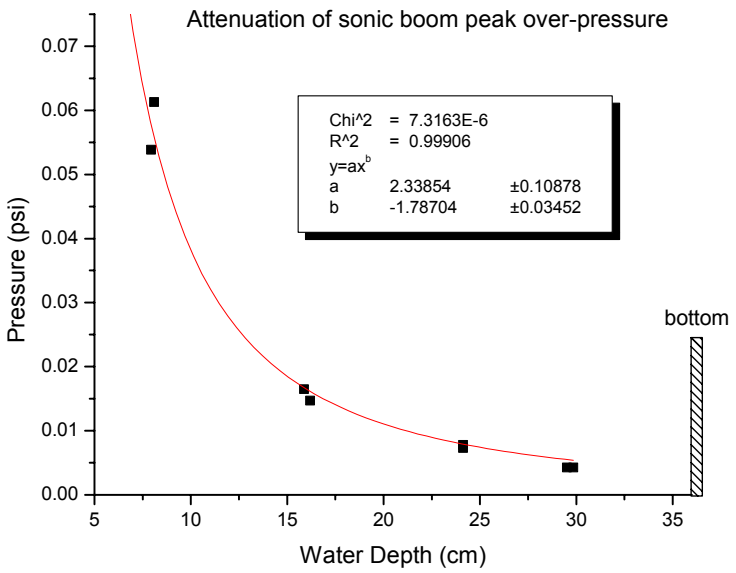

Figure 3: Peak-Peak over-pressure attenuation.

Figure 3 shows a far-field overpressure attenuation of $z^{-1.8}$ consistent with the Sawyer model. Individual overpressure waveforms corresponding to some of the data points in Figure 3 are shown in Figures 4.

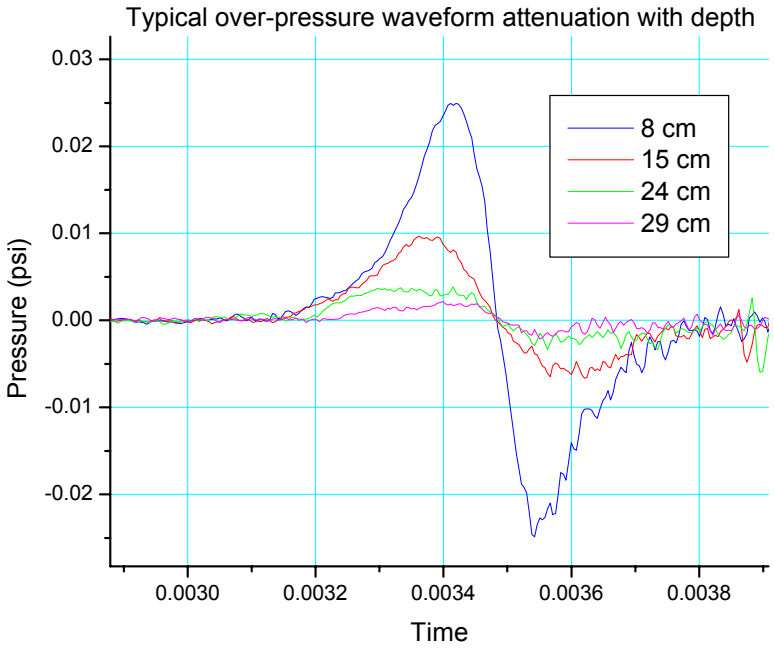

Figure 4: Typical overpressure waveforms.

As can still be seen from Figure 4 (which corresponds to *typical* data taken toward the end of the experimental program after many improvements to the signal to noise ratio were made) as the depth increased the signal to noise ratio of the measurements decreased and at depths below 15 cm it was initially difficult to distinguish the over-pressure signature from the upstream noise without knowing exactly where to look. A systematic study aimed at isolating the source of the noise was initiated. It quickly became clear that the noise had 2 components, the first component was random in nature and associated with the electronics and data acquisition system, the second component proved to be systematic and repeatable and was traced to specific details of the tank/launcher geometry. The random noise was greatly reduced by increasing the charge-coupler gain and improving the overall quality of the wiring, a large isolation transformer and UPS system was installed and used to power all relevant electronics. The repeatable "noise", which appeared as a pre-cursor to the overpressure signatures was shown to correspond to upstream disturbances, possibly related to shock tank interactions. These disturbances propagate faster than the speed of the projectile and arrive at the measurement station before the incident wave signature reaches a detectable level. Appreciable change in the form, phase and amplitude of this pre-cursor were observed when changes were made to the upstream projectile inlet. A smooth vertical wall flush with the upstream end of the tank appeared to work best, but the amplitude of the pre-cursor still limited the maximum depth of useful measurements to 20 cm. Further investigation showed the existence of "sweet spots" at particular longitudinal positions in the tank. These sweet spots were characterized by almost no measurable pre-cursor and were typically 10-15 cm long. It was found that by introducing vertical span-wise sheets of low-density open-cell foam (much like a kelp bed in the coastal ocean) at particular longitudinal positions sweet spots could be induced in a controlled manner. The foam sheets which were typically a 1/2 inch thick were held down with lead weights and did not necessarily need to cover the full span or depth to be effective, they did have a tendency to loose their effectiveness as they became waterlogged after a few days of operation. These foam baffles were never closer than 3 N-wave wavelengths to the piezotrons.

3.2 Wavy water surface

As the primary objective of the project was to determine if we could detect any measurable difference in the underwater signature with and without the presence of surface waves, a large number of ad-hoc tests were done over a wide range of the parameter space at a depth of 10 cm, with the sole objective of qualitatively finding the ringing effect described by Cheng & Lee (2000). Evidence of this effect was soon found see Figure 5 (which shows a *typical* run from the early stages of the experimental program, corresponding to the randomly chosen parameters indicated). The data in Figure 5 is noisy and the pre-cursor mentioned above can be clearly seen. Figure 6 shows data with and without surface waves for one of the later experiments when many ameliorations to the experimental setup and data acquisition system had been completed. A preliminary systematic exploration of the full relevant experimentally obtainable parameter space was subsequently performed. It should be mentioned that due to the large difference in the speed of propagation of the surface waves as compared to the speed of the projectile, the surface wave field can be considered stationary in all cases. As there is no direct synchronization between the wave-generator and the launcher (such synchronization would not be practical in these types of experiments) there is an uncertainty in the actual phase of the waves at the time when the projectile is directly above the sensor. This uncertainty in the surface wave phase is a major source of error in determining the peak amplitude of the wavelet packet envelope, particularly for large values of the surface wavelength where there are fewer wavelets in the envelope and the probability of having one correspond to both the maximum and minimum values of the envelope becomes small.

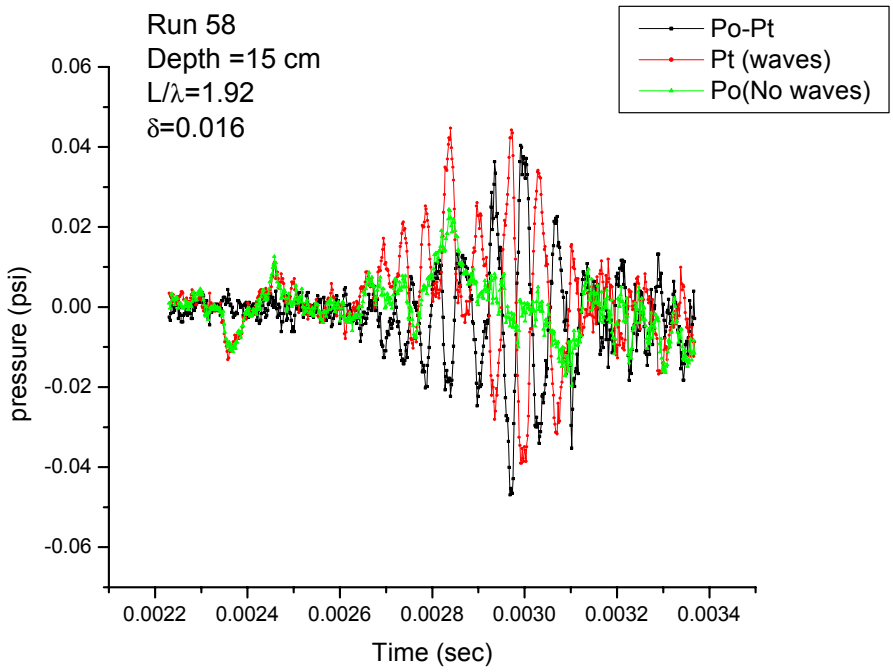

Figure 5: Data with and without surface waves corresponding to a randomly chosen early experiment.

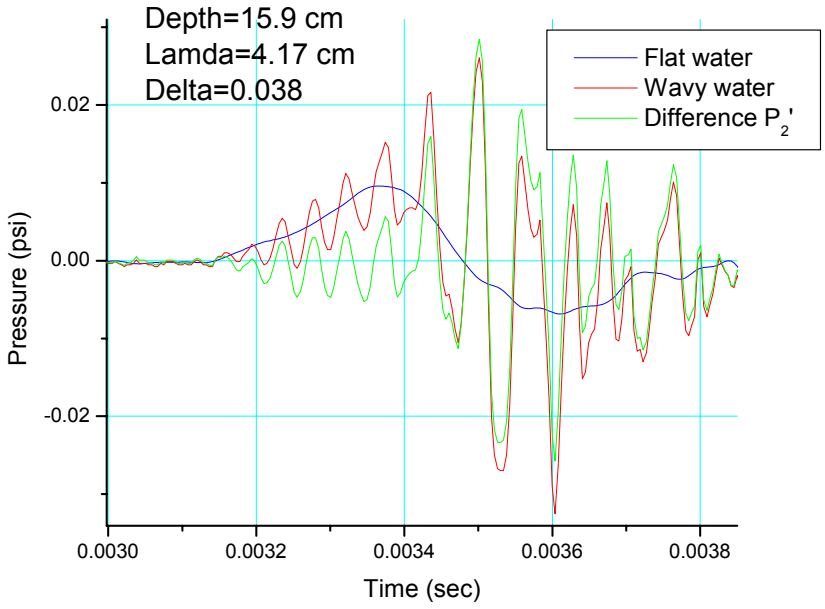

Figure 6: Typical overpressure signal with and without surface waves for one of the later experiments.

By performing multiple ensembles for the same experimental conditions the form of the envelope can be obtained (as the phase for each run is random). This is illustrated in Figure 7 where the signals corresponding to the difference between the wavy and flat-water surface are shown for 2 different ensembles of the same experiment, the true form of the wave packet envelope can be seen.

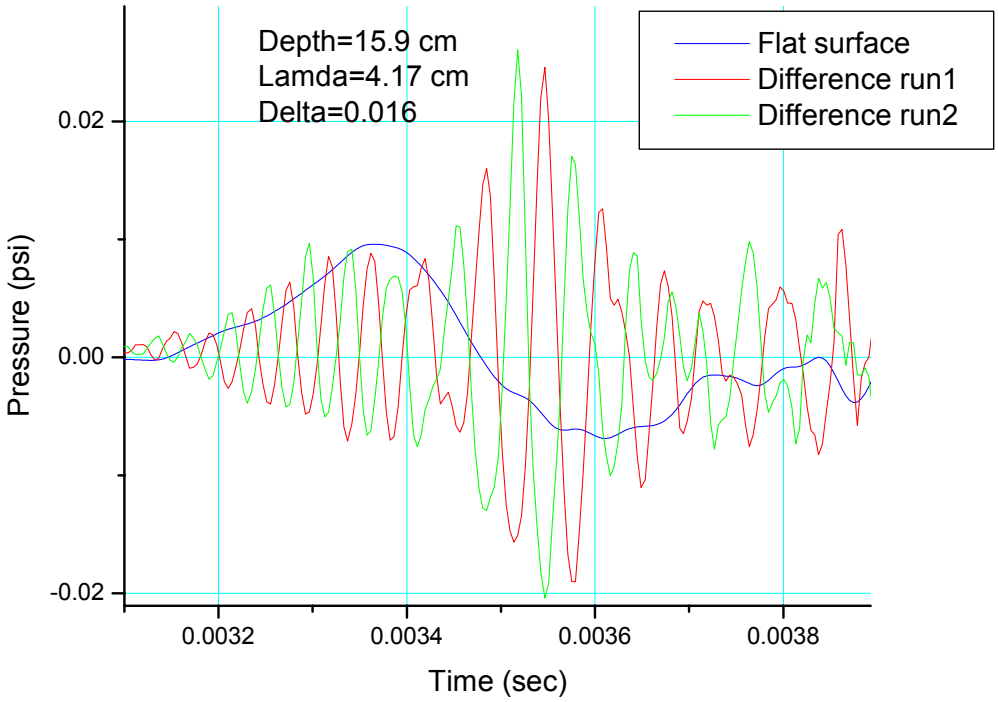

Figure 7: Two different ensembles of the same experiment showing the difference in phase that permits a better resolution of the wave packet envelope.

The generated wave fields

The surface wave fields were generated by forcing the paddle described in Section 2 with a sinusoidal signal generated by a BNC Model 625AT Arbitrary waveform generator, the signal was amplified using a classical Car Stereo amplifier before being fed in parallel to a pair of high performance speakers that were mechanically modified to drive the paddle in phase with their motion. This technique produced surface Capillary-Gravity waves that decayed exponentially with distance away from the paddle. Video images of all surface wave filed used in the experiments were made, these images were used to verify the surface wavelengths λ and as a qualitative check on the overall surface wave field quality, particularly for some of the larger amplitude forcing parameters. An image of a typical wave field is shown in Figure 8.

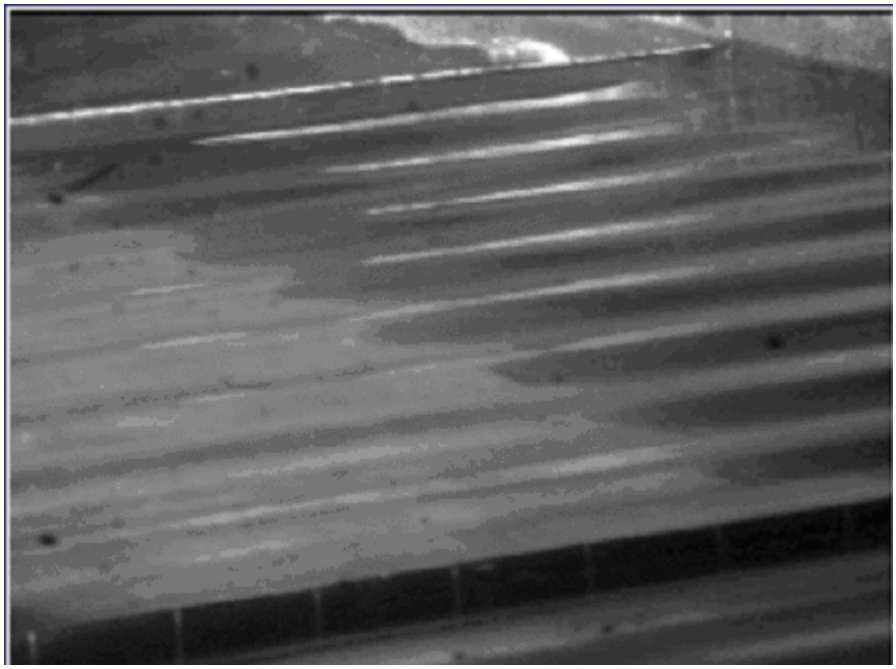

Figure 8: Image of a typical laboratory generated surface wave field.

Surface wave amplitude measurement

As predicted by the theory of Cheng & Lee (2000), it was found that the strength of the phenomena was strongly dependant on the surface wave amplitude. The amplitudes were initially measured using a vertically mounted depth micrometer, which closed a circuit lighting a small LED when it made contact with the water surface. This approach proved laborious and inaccurate due to small variations in the generated wave field and the relatively small amplitudes of the waves, in addition this procedure required the installation of an apparatus that had to be removed before each test. In order to improve on the accuracy of the wave height measurements and to permit dynamic measurements a non-intrusive optical wave height measurement system was subsequently developed.

This optical measurement system consisted of a small laser diode that was aimed at an approximately 25 degree angle such that the beam was reflected from the water surface onto a screen placed just in front of the collector. Any change in the water surface slope would cause the beam to move on the screen. For perfectly sinusoidal surface waves the maximum slope, δ corresponds to the locations of minimum amplitude of the surface wave and for a given surface wavelength, λ the maximum amplitude, A is given by $A=\delta\lambda/2\pi$, as the slope δ corresponds to the maximum deflection on the screen, it suffices to note this maximum deflection and calculate δ based on the geometry of the configuration, see Figure 9.

If the rest position of the laser spot on the screen corresponds to the position indicated by h_2 and angle α and the maximum height with waves present corresponds to position h_1 and angle β, it can be shown that $\beta=\alpha+2\delta$ hence $2\delta=\tan^{-1}(h_1/L)-\tan^{-1}(h_2/L)$. Careful comparisons between the optical and mechanical measurement systems yielded differences of less than 8%.

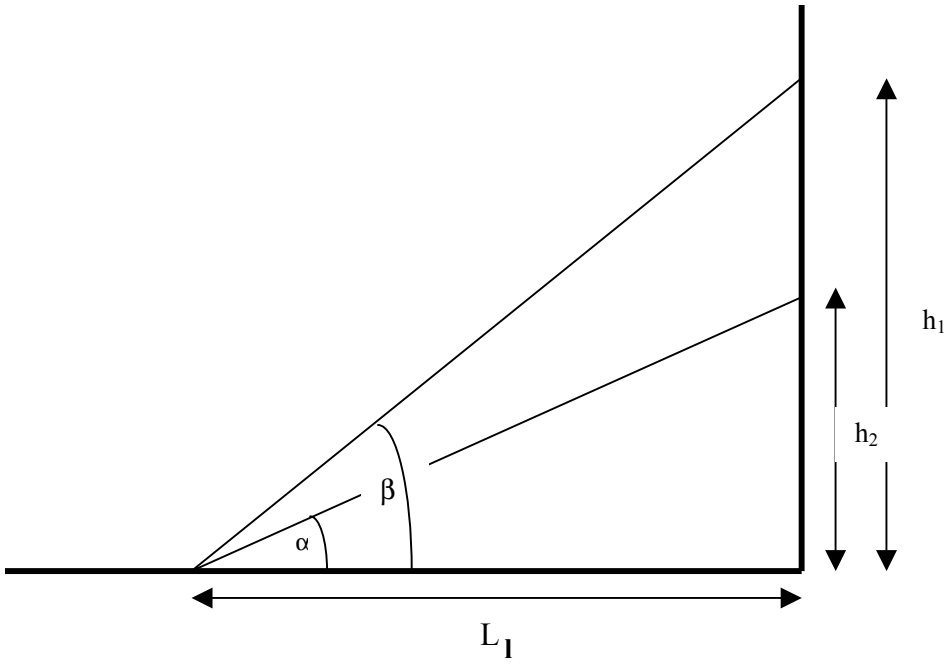

Figure 9: Optical wave height gauge geometry

Characterizing the surface wave fields

Using the optical wave height gauge the typical wave heights at any location in the tank could be quickly measured. Due to strong viscous/capillary effects at the relatively small scale of the laboratory setup, the surface waves exhibited significant decay in amplitude away from the generating paddle. Figure 10 shows the wave half height as a function of distance behind the wave-generating paddle for forcing frequencies of 5, 6 and 7 Hz corresponding to surface wavelengths λ of 3.1, 4.2 and 6.0 cm respectively and constant input voltage.

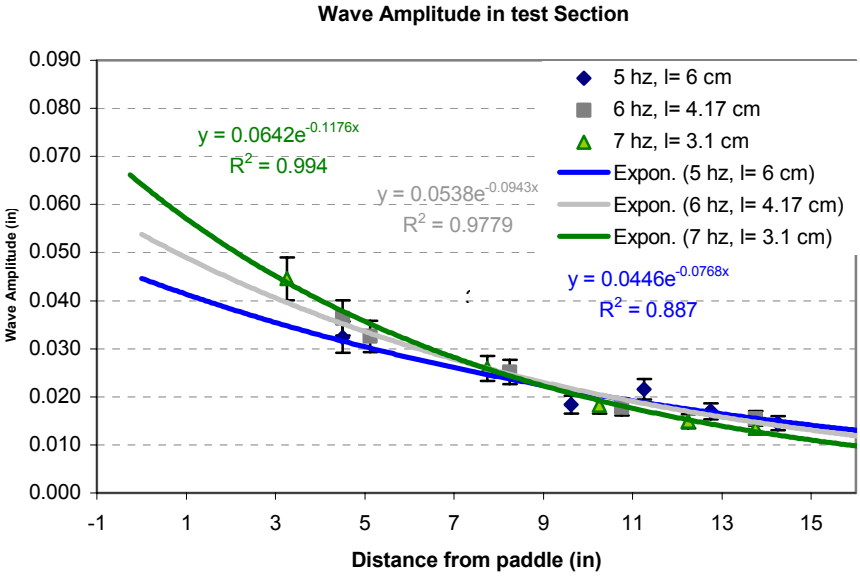

Figure 10: Surface wave height decay away from the paddle.

Figure 10 shows that the shorter wavelength waves with larger slopes have larger decay exponents making the generation of a constant wave height wave field more difficult. As the desired wavelengths were determined mainly be the length of the projectiles being used (which were already the longest feasible projectiles) some effort was made to try and limit the decay of the surface wave field in order to obtain a more constant amplitude wave train above the piezotrons. It was decided to add an upstream stationary paddle that would reflect wave energy downstream creating a region of "standing waves". The effects of the paddle are shown in Figure 11 for λ =4.17 cm, here the parameter delta is used for the wave amplitude $\delta=A/\lambda$, where A is the measured half height of the waves and λ is their wavelength.

The stationary paddle can be seen to be effective in reducing the exponent of the decay but its presence was found to cause some additional noise and more importantly the wave fields generated with the stationary paddle installed were found to be rather "chaotic" in nature due to the reflected waves not being perfectly in phase with the incident wave trains, such that the amplitude of the waves directly above the piezotrons had a much larger variability, hence making exact determination of the wave amplitude at the instance of the projectile over-flight impossible. For the above reasons the stationary paddle was NOT used for the data presented in this report.

The addition of small quantities of surfactants was found to further decrease this amplitude decay, see Figure 12, but its effectiveness deteriorated quickly with time making it difficult to repeat consistently.

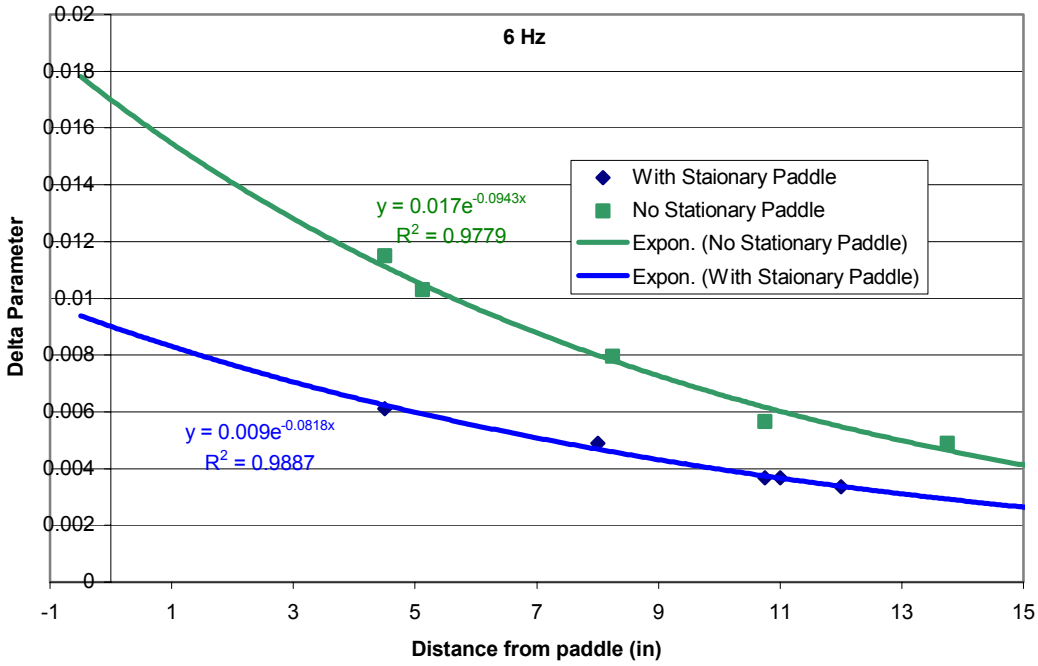

Figure 11: Effects on upstream stationary paddle on surface wave amplitude decay.

The constraint of having to add the surfactant immediately before each run was determined to undermine some of the implemented testing safety procedures and the final procedure used involved adding a small quantity of surfactant several minutes before each run and cleaning the dust from the water surface regularly. Qualitative diagrams of the measured surface wave amplitudes for 2 of the typical surface wavelengths used in the majority of the experiments are shown in Figures 13 and 14. Once again it can be seen that the smaller values of λ are associated with larger decay exponents, this will be discussed later when the dependence of P_2' on λ is examined.

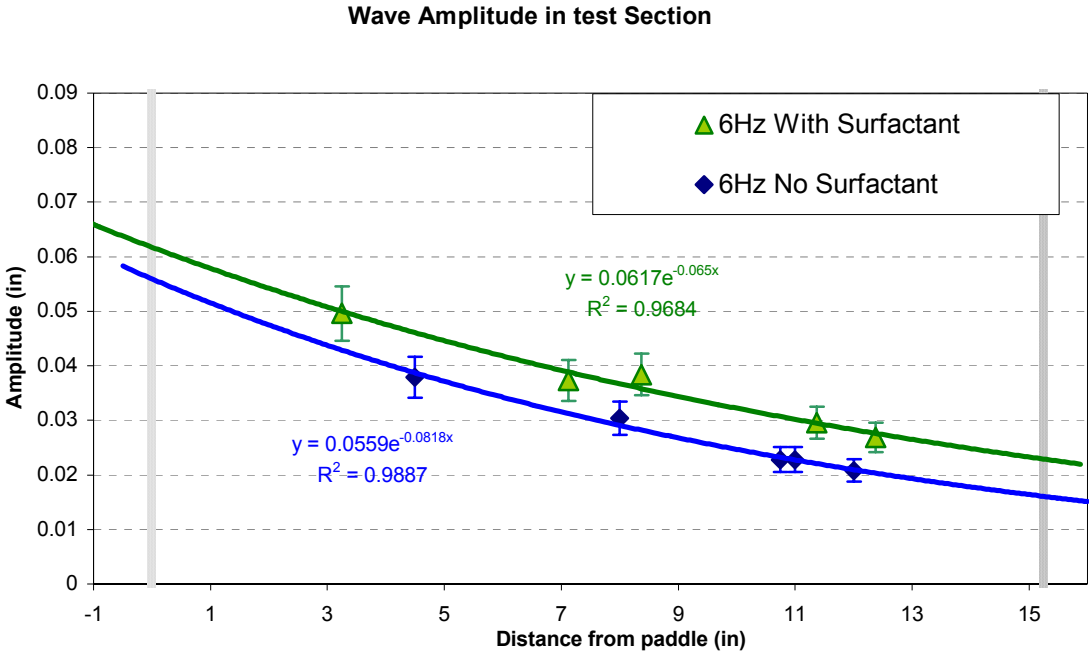

Figure 12: Effects of surfactants on surface wave amplitude away from paddle.

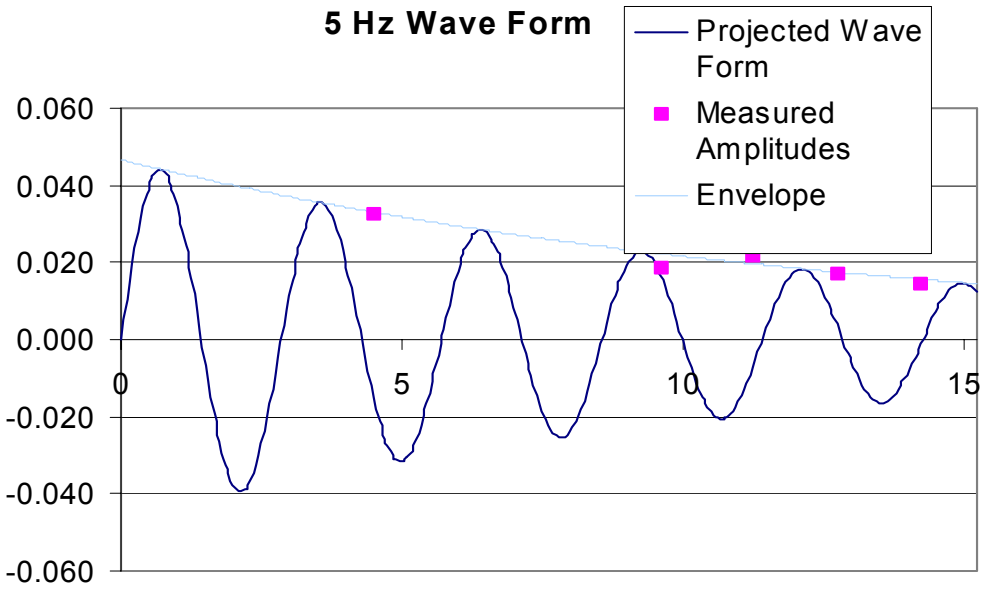

Figure 13: Projected surface waveform decay with distance from paddle for λ=3.1 cm.

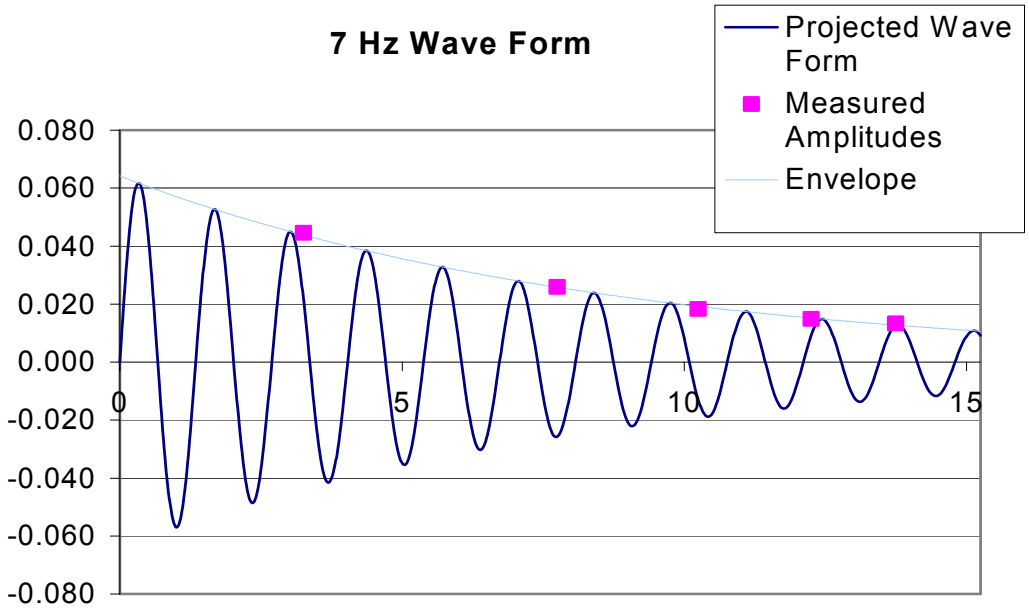

Figure 14: Projected surface waveform decay with distance from paddle for λ=3.1 cm.

The importance of delta

The surface wave amplitudes are characterized by their slope δ=A/λ, the analysis of Cheng and Lee (2000) involves a surface wave train where δ is constant for O(10) wavelengths in the vicinity of the sensors. According to Cheng and Lee the peak-peak amplitude of the envelope P_2', (P_2' =P_{total} (with waves)-P_o(flat water)) should increase linearly with δ (up to some saturation value, or critical wave slope to Mach angle ratio). As δ in these experiments decreases exponentially away from the wave generating

paddle and as the region of surface influence increases with the depth of the measurements, only measurements made at relatively shallow depths can be expected to have a moderately constant surface wave train amplitude influence. Figure 15 shows P_2' as a function of δ for a depth of 8.1 cm and λ=4.17 cm. At depths of less than L′~8cm we are typically in the near field for both the flat water and the wavy water attenuations. As these experiments are aimed primarily at verifying the far-field attenuation laws for both the flat and wavy air/water interfaces, data taken in the near field (z<L′) where the surface wave trains influencing P_2' are relatively constant in amplitude are not useful for this particular objective. For depths greater than L′ where the surface influence consist of a region with increasing variation in δ with depth, we expect significant deviation from a linear dependence of P_2' on δ. This is illustrated in Figure 16, where P_2' is shown verses δ for 3 different depths.

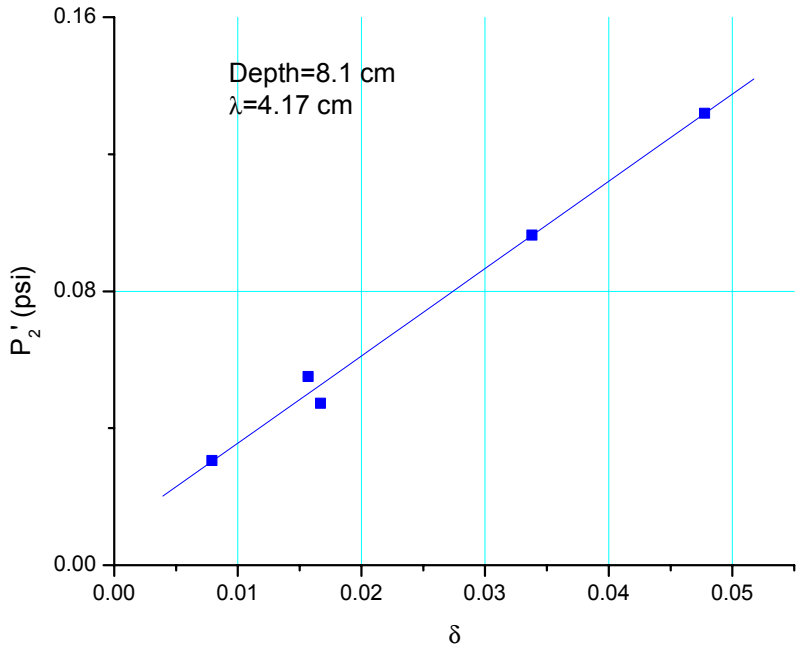

Figure 15: Linear dependence of P_2' on measured delta for shallow depths.

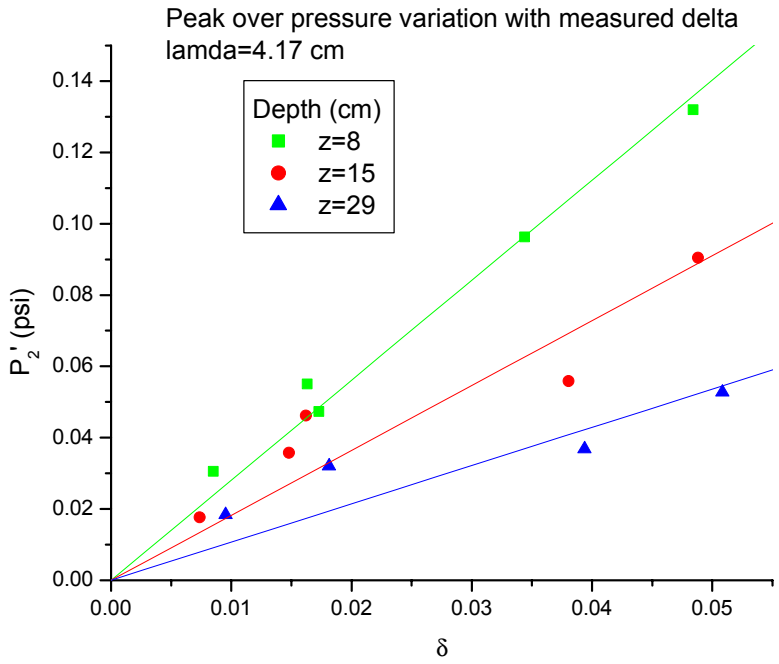

Figure 16: P_2' verses δ for different depths

Some comments are in order here on the measurement of the peak P_2' amplitudes from the pressure time traces. As can be clearly seen from Figure 7, the amplitude of the P_2' wave packet is asymmetric around the zero crossing of the flat-water over-pressure signature. This asymmetry is due directly to the variation in δ on the free surface above the sensors. The surface waves upstream of the piezotron locations have larger amplitudes than those on the downstream side. The values of δ used in Figures 15 and 16 are measured perpendicularly above the piezotrons and do represent some typical value but, due to the exponential decay of δ, they are neither average values, nor is their representation constant when either one of the depth, the surface wavelength λ or δ itself is varied. When determining the maximum value of the P_2' envelope from these time traces, the peak values are used regardless of their location in the envelope. The precise location is always noted with the intension of using the data from Figures 10-14 to determine the approximate value of δ for the particular surface wave corresponding to the peak amplitude sub-wavelet within the envelope that gave this maximum value for P_2'.

The attenuation of P_2'

The theory of Cheng and Lee (2000) predicts a far-field 2D cylindrical spreading type attenuation of P_2' with depth, corresponding to, $P_2' \sim \varepsilon\delta/z^{1/2}$ where ε is the overpressure ratio $\varepsilon = P'/P_a \sim 0.1$. Figure 17 shows $P_2'/\varepsilon\delta$ plotted against the normalized depth in N-wave signature lengths L′. A best-fit line shows a decay as $z^{-.55}$ not far from the $z^{1/2}$ predicted by the theory.

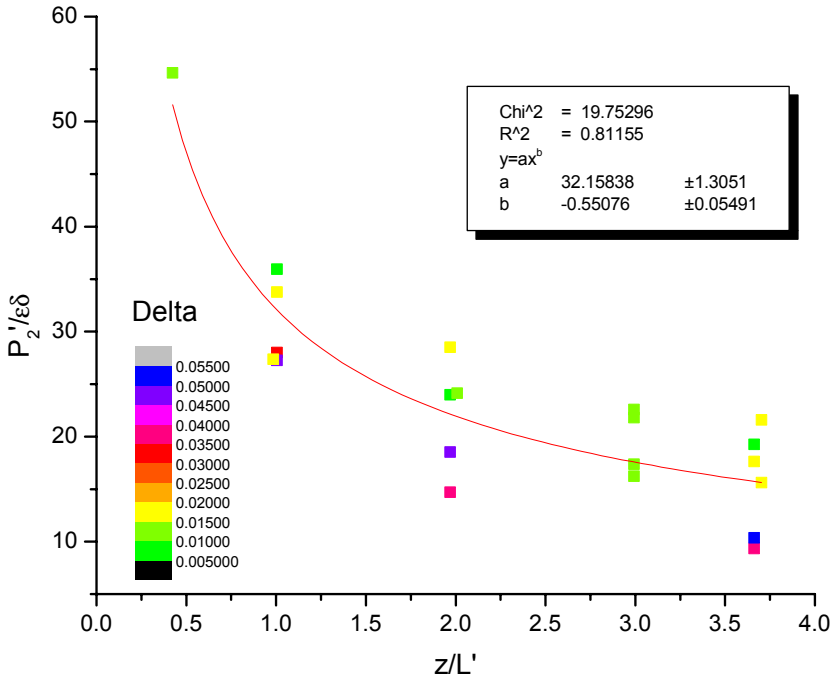

Figure 17: Normalized attenuation of P_2'.

The data in Figure 17 can also be represented by normalizing P_2' by the measured values of P_2' at one signature depth. Such normalization is justified as the predicted attenuation law is only valid in the far field, which corresponds roughly to depths greater than one signature. This is shown in Figure 18, where slightly better collapse of the data is observed and there is slightly better agreement with the theory.

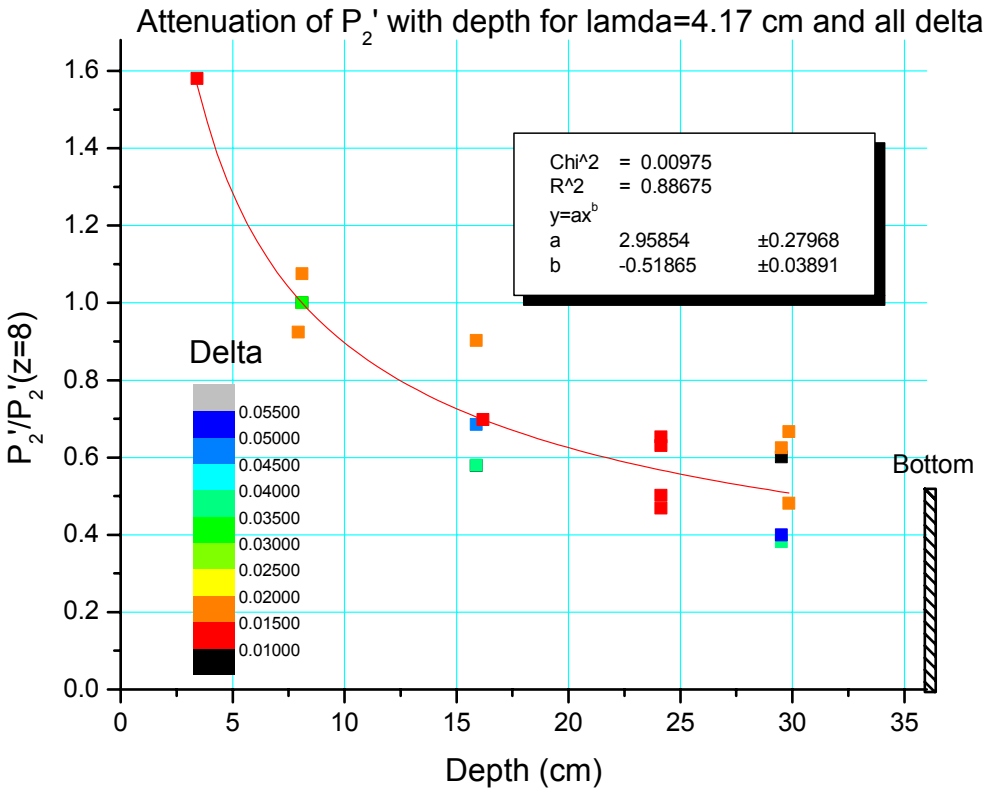

Figure 18: P_2' normalized by the measured P_2' at z=8 cm (1 signature depth).

Individual time traces of P_2' are shown in Figure 19(a,b) for 4 different depths, it can be seen that as the depth increases the width of the envelope of P_2' also increases and a larger number of wiggles can be seen. The asymmetry in the envelope is clearly seen to increase with depth as the area of surface influence increases. By using Figure 10 it is possible to *estimate* the local δ for each wiggle in Figure 19, for the depth of 29 cm the δ measured directly above the probes is estimated to be only about 65% of the δ primarily responsible for the largest amplitude wiggle to the right in Figure 19 which occurs about 5 inches downstream of the sensor location. It could be this particular wiggle that is responsible for the measured peak amplitude of P_2' in figure 18. This effect will apply in a similar fashion to each measured value of δ.

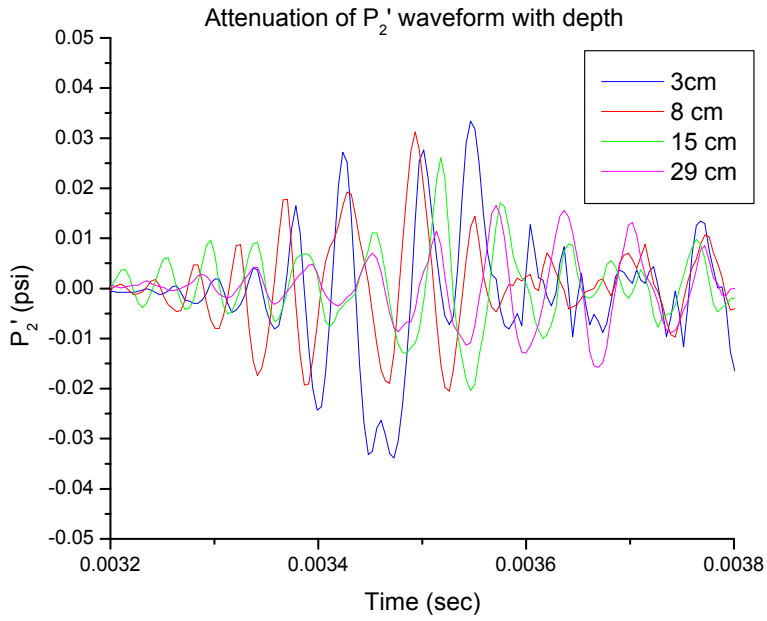

(a)

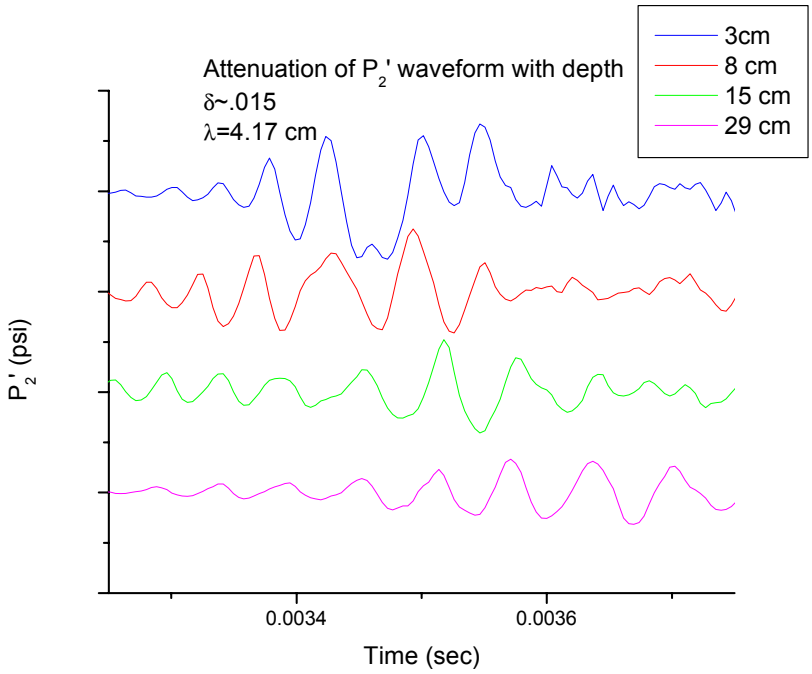

(b)

Figure 19: (a)Pressure time traces of P_2' for 4 different depths, all else constant. (b) same data displaced .05 psi in y.

Dependence on the surface wavelength λ

The development of the P_2' phenomena is strongly dependent on λ and as predicted by the theory of Cheng and Lee there is a specific range of L'/λ where the phenomenon is observed. Measurements were made for a range of L'/λ corresponding specifically to λ 's of 1.53, 1.87, 2.36, 3.1, 4.17, 6.0, 9.46, 16.8 and 29.5 cm. The dependence of the effective δ on both λ and the depth make it difficult to isolate the most receptive value of L'/λ without first decoupling the effects of δ, such an analysis is presently in progress and using the technique described briefly above should be viable, but time consuming. Nonetheless some preliminary observations can be made.

A crude estimate of the optimum ratio L'/λ can be obtained from some of the preliminary data taken with the first generation (wooden, vertically oscillating) wave paddle and based on mechanical measurements of δ. This data is presented in Figure 20, and shows an optimum L'/λ of about 2 (although this depends on δ). Some typically plots showing the relative contributions of the total measured pressure P', the flat water component P_1' and the wavy water component P_2' are shown in Figures 21-29. We can see from Figures 21 and 29 (pressure units are psi*5.5) that we have almost exhausted the full range of λ for which any strong interactions are present.

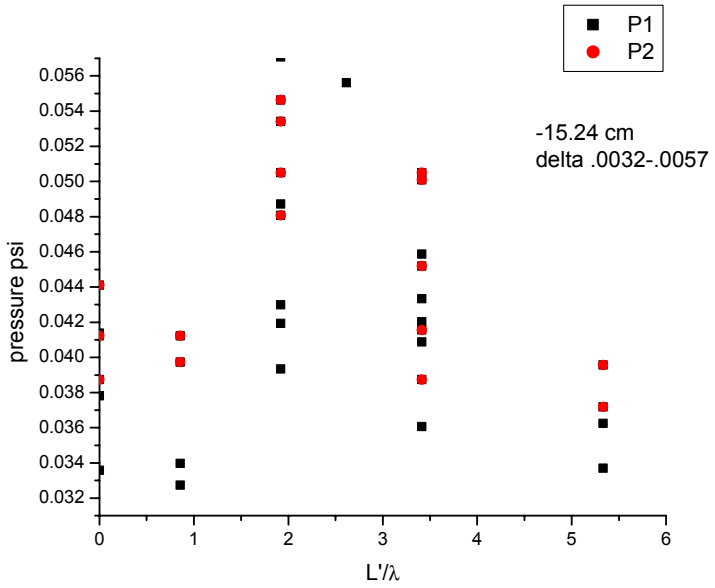

Figure 20: Preliminary peak measured pressure for probes at 2 different streamwise positions vrs. λ/L' based on older data acquisition and laboratory setup.

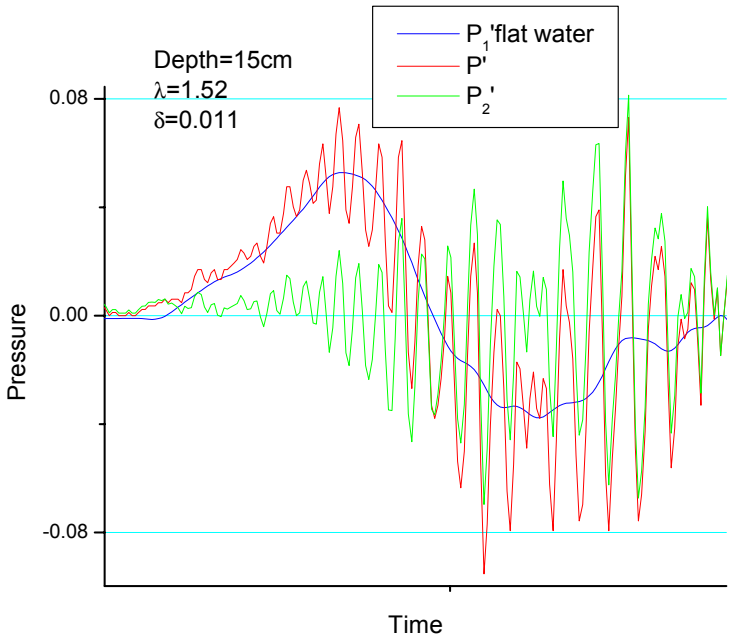

Figure 21: Newer data for λ=1.52 cm and parameters indicated.

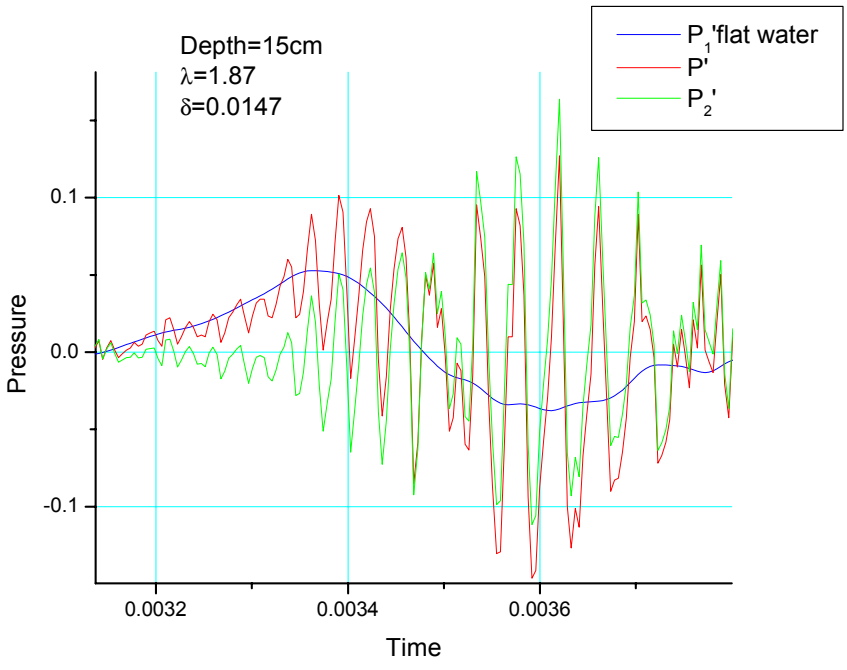

Figure 22: Newer data for λ=1.87cm and parameters indicated.

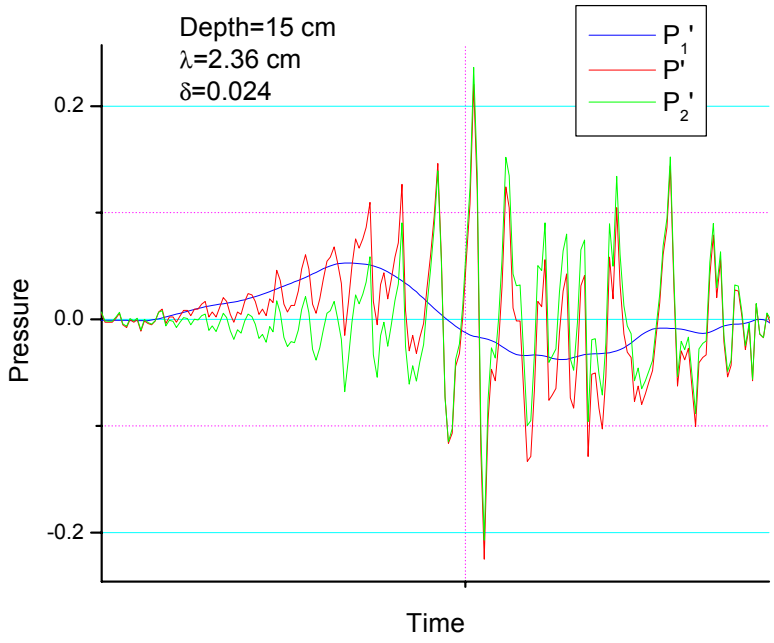

Figure 23: Newer data for λ=2.36 cm and parameters indicated.

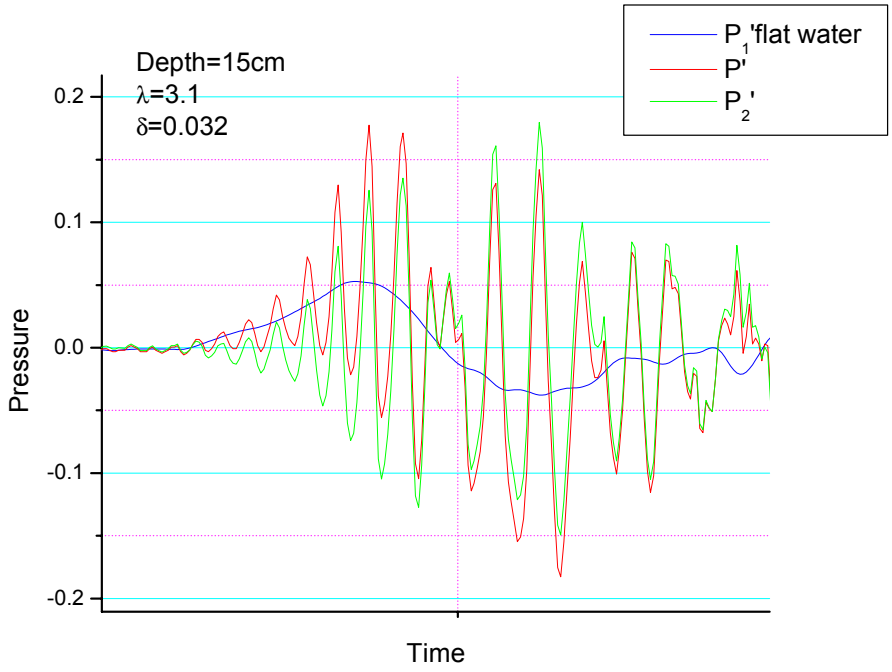

Figure 24: Newer data for λ=3.1 cm and parameters indicated.

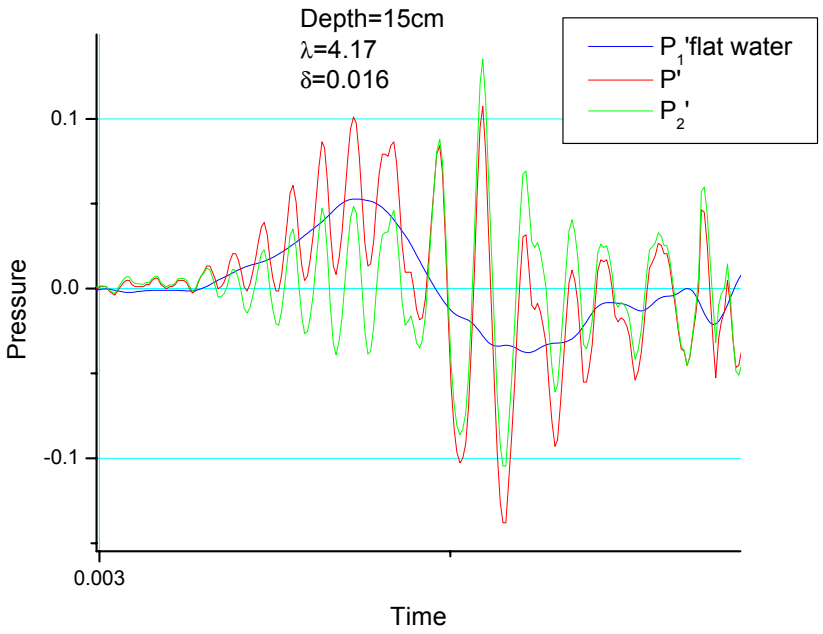

Figure 25: Newer data for λ=4.17 cm and parameters indicated.

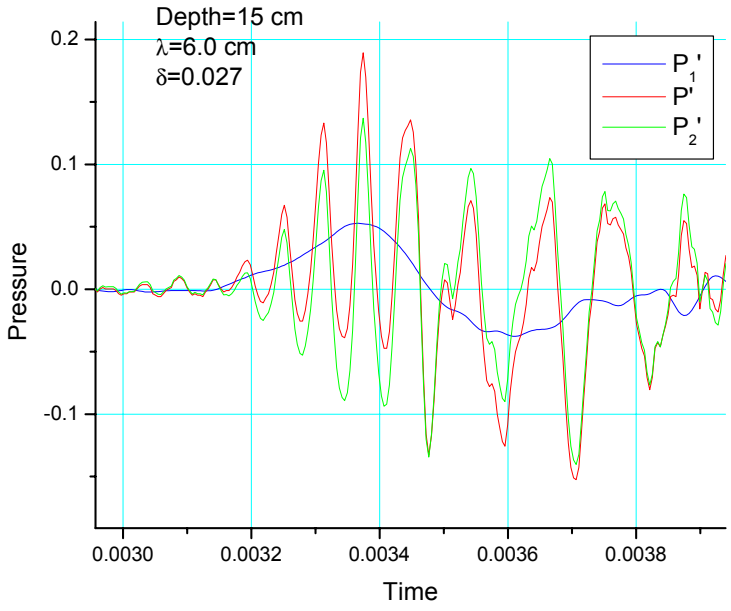

Figure 26: Newer data for λ=6.0 cm and parameters indicated.

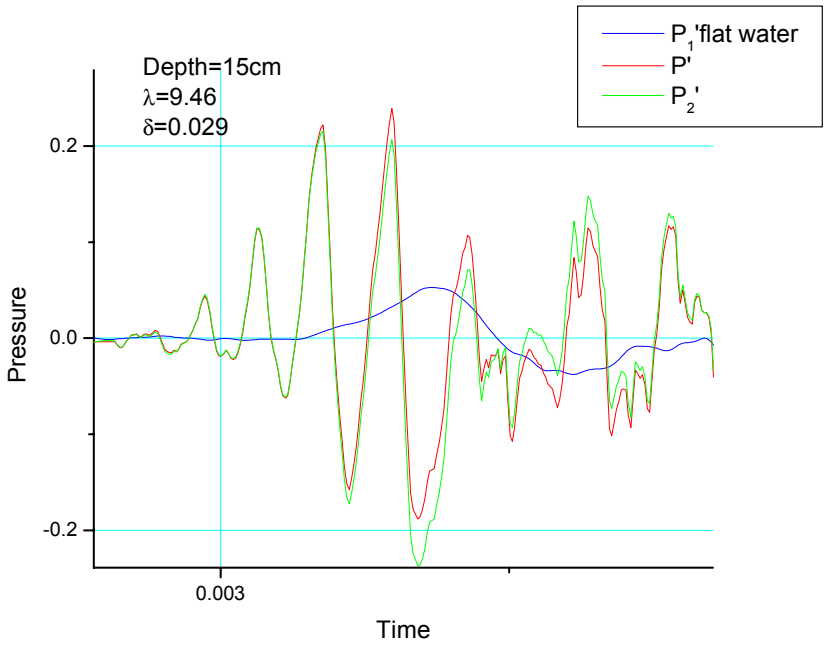

Figure 27: Newer data for λ=9.46 cm and parameters indicated.

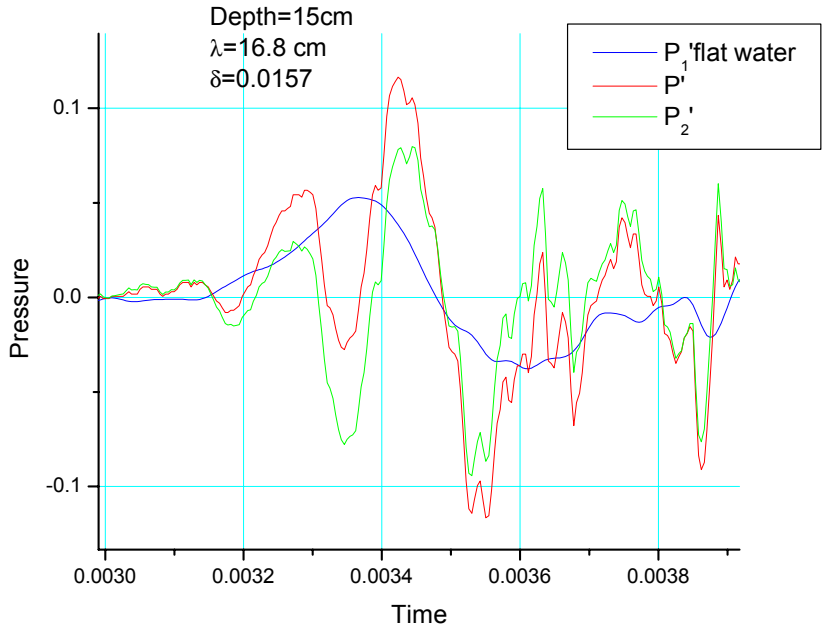

Figure 28: Newer data for λ=16.8 cm and parameters indicated.

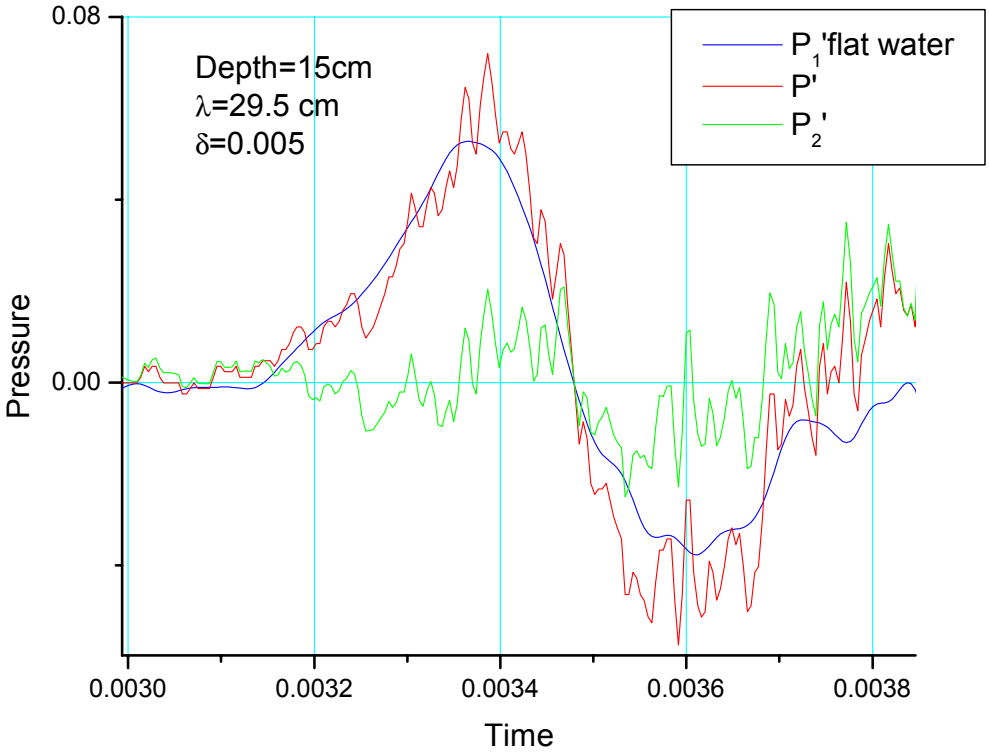

Figure 29: Newer data for λ=29.5 cm and parameters indicated.

Inclined wave trains

Measurements were made for surface wave trains that were inclined to the flight path at an angle of 15 degrees. This was facilitated by inclining the entire tank with respect to the fixed flight path, care was taken to ensure that the axis of rotation was centered on the principal piezotron which effectively did not change location during the rotation process. Figure 30 shows a comparison of the P_2' signals for the plane and inclined cases. A small difference in frequency can be seen which corresponds roughly to the effective increase in the projected wavelength λ for the inclined case.

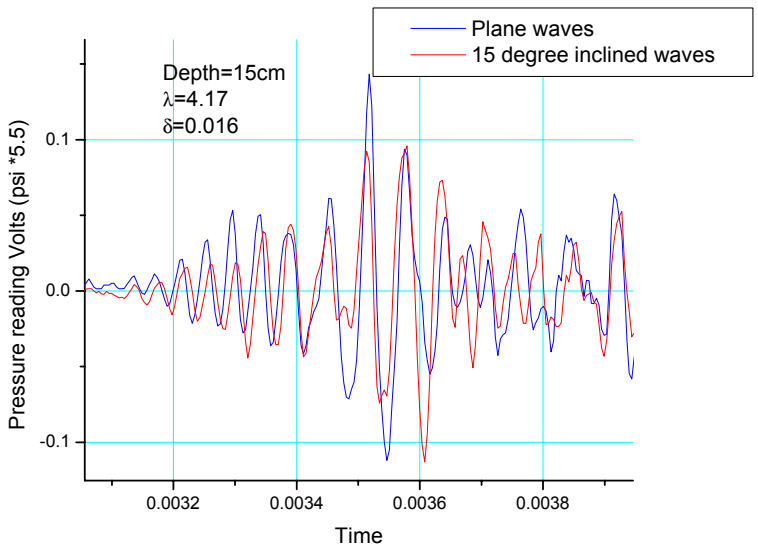

Figure 30: Effects of inclined surface wave trains.

4. Discussion and Conclusions

Several different series of measurements were made during the 8 months of testing. Due to continuing development and improvements in both the data acquisition and other measurement systems, each series of experiments was treated independently and typically the older data was quickly exploited then discarded once the desired changes (improvements) were achieved. This approach provides adequate verification of any questionable results under slightly different experimental conditions and contributes to the overall robustness of these results.

These experimental results which were achieved through determined laboratory efforts dedicated to obtaining the highest quality data possible, show conclusively that the theory of Cheng and Lee (2000), the one half power overpressure attenuation rule in particular, is valid at the laboratory scale. Further, the Sawyer model has been experimentally verified to large depths for the first time. Of interest are the wavelet frequencies and the fore-to-aft frequency shift found in experiment, which are also in accord with Cheng and Lee's analysis. Many comments can be made in hindsight as to potential improvements in the overall experimental design and procedures, many new questions have also arisen from this research, detailed comments on these thoughts will be left for reflection in subsequent studies.

Acknowledgements

We would like to acknowledge the invaluable assistance of Noor Sahota who helped in all the initial construction and testing, Philippe Kassouf who helped particularly in the measurement of the surface wave fields and in some of the data post processing. Lengthy discussions with Professor H. K. Cheng during the course of the experiments has greatly added to the overall quality and direction of this research. The enthusiastic participation of John R. Edwards in the laboratory program has helped add both general direction and motivation throughout this work.

References

Intrieri, P. F. and Malcolm, G. N., "Ballistic range Investigation of Sonic-Boom Overpressure in Water," AIAA J., vol. ll, no. 4, pp. 510-516 (1973).

Water, J., "Penetration of Sonic Energy into the Ocean: An Experimental Simulation," Noise & Vibration Control Engineering (ed. M. Croker), Proc. Noise Control Conf. Purdue Univ., July 11- 16, 1971, pp. 554-557 (1971).

Cheng, H. K. and Lee, C. J., "Sonic Boom Noise Penetration Under a Wavy Ocean: Part I Theory," Univ. Southern Calif. Dept. Aerospace & Mechanical Eng., USC AME Report 11-11-00 (2000); documented on web site <http://www-bcf.usc.edu/-hkcheng>.

Desharnais, F. and Chapman, D. M. F., "Underwater Measurement and Modeling of a Sonic Boom," Abstract in J. Acoust Soc. Am., vol. 04, no. 3, pt. 2, p. 1848 (1998).

Sohn, R. A., Vernon, F. Hildebrand, J. A. and Webb S. C., "Field Measurement of Sonic Boom Penetration into the Ocean," J. Acoust. Soc. Am. Vol. 107, pt. 6, pp. 3073-3082 (2000).

Sawyers, K. H., "Underwater Sound Pressure from Sonic Boom," J. Acoust. Soc. Amer., vol. 44, no. 2, pp. 523-524 (1968).